Advances in Research
6(3): 1-14, 2016, Article no.AIR.22738
ISSN: 2348-0394, NLM ID: 101666096

SCIENCEDOMAIN *international*
www.sciencedomain.org

PID Control Design of Sideslip Angle for a Fixed-Wing Mini-UAV

B. K. Aliyu[1*], A. A. Petinrin[1] and J. A. Adewumi[1]

[1]Centre for Space Transport & Propulsion (CSTP), Epe, Lagos-State, Nigeria.

Authors' contributions

This work was carried out in collaboration between all authors. Author BKA designed the study, simulated and analyzed all plants, controllers in MATLAB/Simulink and Maple. He also wrote the first draft of the manuscript. Author AAP validated all MATLAB/Simulink and Maple results. Author JAA handled DATCOM computations, re-checked MATLAB/Simulink results and managed literature search. All authors read and approved the final manuscript.

Article Information

DOI: 10.9734/AIR/2016/22738
Editor(s):
(1) Akash Dixit, Department of Mechanical Engineering, Oakland University, USA.
Reviewers:
(1) P.A. Murad, Vienna, Virginia.
(2) Manoel F. Borges, Sao Paulo State University, Brazil.
(3) Basil Hamed, Islamic University of Gaza, Palestine.
Complete Peer review History: http://sciencedomain.org/review-history/12604

Original Research Article

Received 23rd October 2015
Accepted 24th November 2015
Published 9th December 2015

ABSTRACT

Sideslip angle is one of the state variables in the lateral state-space dynamics of an Unmanned Aerial Vehicle (UAV). Large asymmetric aerodynamic loads can be induced on a UAV's fuselage, even at zero sideslip. For steady and level flight, this angle must be controlled. To control the sideslip angle, a mathematical model for the UAV is required using static and dynamic aerodynamic as well as cross-term coefficients. Aircraft Digital Datcom was used to estimate the UAV's aerodynamic coefficients, aerodynamic stability and control derivatives from its physical geometry. The challenge for a control engineer is the choice of transfer function (plant) to be used for sideslip angle controller design in an autopilot system. Since both the lateral model and it reduced form; Dutch Roll (DR) approximated model have sideslip angle as a state variable. In this study, the pitch plane is ignored as well as cross-terms in the moments of inertia. Dutch Roll is focused upon firstly; we investigated the dynamics characteristics of both models. Secondly, sideslip angle transfer functions obtained from both the lateral and DR approximated models were compared. The eigenvalues, natural frequencies, damping ratio, period and number of cycle to

**Corresponding author: E-mail: aliyu_bhar@yahoo.com;*

damp to half amplitude of the Dutch roll mode in the lateral dynamics are about the same with those of the Dutch roll approximated model. Steady state values and open-loop step responses computed in MATLAB & Maple differ in magnitude and direction on the Cartesian plane. Despite the limitations of this initial effort, Proportional-Integral-Derivative (PID) controllers were designed in MATLAB/Simulink for all transfer functions. Design results analysed gives intuitive and informed design choice for autopilot gains for the sideslip angle control.

Keywords: UAV; PID control; DIGITAL DATCOM; MATLAB/Simulink; Maple®; lateral dynamics.

1. INTRODUCTION

Unmanned Aerial Vehicles (UAVs) have proven their usefulness in military reconnaissance in recent military conflicts [1]. Their practical applications have been expanding to more than military uses. Various sizes of UAVs are designed for different levels of performance depending on their application. UAVs can be categorized into four different groups: large, medium, small (mini), and micro.

The military has shown the most recent interest in mini-UAVs for many reasons. The mini-UAV has a wing span of less than 2 m and a gross weight of less than 100 kg. It is much more portable than its large counterparts and requires only one operator. Mini-UAVs can assess ground targets at a closer range without being detected. Therefore, most mini-UAVs use electric motors as a propulsion system, which allows for a stealthier and more reliable flight with little engine failure. Also a mini-UAV is less expensive and can be considered a disposable asset. This factor allows pilots to navigate hostile areas and focus on their primary mission, rather than plane recovery. In addition to military applications, size and cost advantages are attracting civilian and private uses. Therefore, mini-UAVs are most suitable for use in non-military applications because they are less expensive and less dangerous [2].

It has long been recognized that asymmetric vortex shedding can occur on bodies of revolution at high angles of attack. The major problem is that at large angles of attack, a vortex is formed on one side or another in a random or unknown fashion especially with no sideslip. This analysis will not use large angles to simplify this phenomenon.

Large asymmetric loads can be induced on the body itself, even at zero sideslip [3]. Experimental results have shown that the vortex-induced side force can be as high as, or exceed, the normal force [4]. In the angle-of-attack range where vortex shedding is asymmetric the axial flow component is still sufficient to produce steady vortices. However, the vortex pattern is asymmetric, producing a side force and a yawing moment, even at zero sideslip. This side force is the result of surface pressure imbalances around the fore-body of the aircraft caused by an asymmetric fore-body boundary layer and vortex system [5]. As such, instability can be induced on the UAV and loss of control will be imminent.

To autonomously control the UAV sideslip angles and we require firstly, a lateral dynamics mathematical model and secondly, a control algorithm. The ability to control the UAV's sideslip angle response to match command parameters requires an autopilot. This ability is largely determined by the performance of the control algorithm implemented by the autopilot software. All autopilots reviewed for UAVs state that their control algorithm uses the well-established proportional, integral, derivative (PID) controller [6-9]. The Proportional-Integral-Derivative (PID), controller dates back to 1890s, with the first practical example from 1911 [10].

In this study, we are careful enough to show that the transfer function for sideslip angle from the lateral dynamics model differs from those of a reduced Dutch Roll model. Hence, PID control gains will differ in the implemented autopilots system, which could mar the autopilot system capability to control sideslip angle during flight.

The mini-UAV, Ultra Stick 25e chosen for this research is commercially available and serves as the primary flight test vehicle for the University of Minnesota UAV flight control research group. The UltraStick 25e is a fixed-wing, radio controlled aircraft. It is equipped with conventional elevator, aileron, and rudder control surfaces. The aircraft is powered by an electric motor that drives a propeller. These will be used for aerodynamic changes as well as altering thrust with altering the current on the electric motor employed within this simulation.

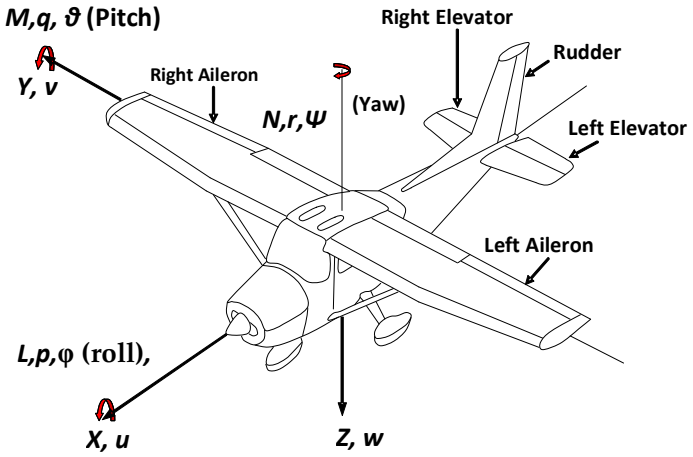

Fig. 1. 6DoF variables of the Ultrastick 25e mini-UAV

The basic physical characteristics of the UAV are as outlined in Table 1. Also, presented in the table are the associated with calculated moments of inertia.

Table 1. UAV parameters

Parameter	Description	Value and units
A	Wing Reference Area	0.31 m^2
b	Wing Span	1.27 m
$\bar{c}$	Wing Chord	0.25 m
m	Gross weight	1.9 kg
m_c	Mass of Payload	0.25 kg
m_T	Take off mass	2.15 kg
I_x	Roll moment of inertia	0.07151 $kg.m^2$
I_y	Pitch moment of inertia	0.08636 $kg.m^2$
I_z	Yaw moment of	0.15364 $kg.m^2$
I_{xz}	Product of inertia	0.014 $kg.m^2$

The UAV will be assumed to be symmetrical, which means cross-coupling inertial effects that may or may not influence yaw-roll and Dutch roll are assumed negligible. This assumption is felt valid during the preliminary design stages as in this study. We are yet to fly the UAV, and we expect it to exhibit these cross coupling effect because the body structure can never be perfectly symmetrical.

This paper is organized as follows: A lateral fixed-wing aircraft flight dynamics model structure is presented from a six-degree-of-freedom (6DoF) equation of motion (EoM) standpoint in 2.0. Hence, open loop system dynamic analysis is done. Also, actuator dynamic model for the aileron and rudder is presented. Section 3.0 introduces an Autopilot system and the PID control algorithm. Also, the designed sideslip angle controllers are presented. In section 4.0, all results were discussed.

2. LATERAL FIXED-WING AIRCRAFT FLIGHT DYNAMICS

The fundamental goal of flight dynamics modelling is to represent the flight motion numerically for a given input and output, as close to the flight motion in the real world as the application requires. All flight dynamics models are based on the mathematical model derived from Newtonian Physics. From Newton's second law, an aircraft's motion in its six-degrees-of-freedom (DOF) can be described by a system of non-linear first order differential equations.

These equations of motion served as the fundamental for almost all flight dynamics model.

Twelve states are required to describe the aircraft rigid-body dynamics, these are: three inertial positions (X, Y, Z), three body-axis velocities (u, v, w), three attitude angles (θ, φ, Ψ), and three body-axis angular rates (p, q, r). The coupled (longitudinal and lateral dynamics) 6DoF equation of motion for a rigid aircraft is given as [11];

$$m\dot{u} - \overset{o}{X}_u u - \overset{o}{X}_v v - \overset{o}{X}_{\dot{w}} - \overset{o}{X}_w w - \overset{o}{X}_p p - \left(\overset{o}{X}_q - mW_e\right) q - \overset{o}{X}_r r + mg\theta\cos\theta_e = \overset{o}{X}_\xi \xi + \overset{o}{X}_\eta \eta + \overset{o}{X}_\zeta \zeta + \overset{o}{X}_\tau \tau \quad (1)$$

$$-\overset{o}{Y}_u u + m\dot{v} - \overset{o}{Y}_v v - \overset{o}{Y}_{\dot{w}} \dot{w} - \overset{o}{Y}_w w - \left(\overset{o}{Y}_p + mW_e\right) p - \overset{o}{Y}_q q - \left(\overset{o}{Y}_r - mU_e\right) r - mg\phi\cos\theta_e - mg\psi\sin\theta_e = \overset{o}{Y}_\xi \xi + \overset{o}{Y}_\eta \eta + \overset{o}{Y}_\zeta \zeta + \overset{o}{Y}_\tau \tau \quad (2)$$

$$-\overset{o}{Z}_u u + \overset{o}{Z}_v v + \left(m - \overset{o}{Z}_{\dot{w}}\right)\dot{w} - \overset{o}{Z}_w w - \overset{o}{Z}_p p - \left(\overset{o}{Z}_p + mU_e\right) q - \overset{o}{Z}_r r - mg\theta\sin\theta_e = \overset{o}{Z}_\xi \xi + \overset{o}{Z}_\eta \eta + \overset{o}{Z}_\zeta \zeta + \overset{o}{Z}_\tau \tau \quad (3)$$

$$-\overset{o}{L}_u u - \overset{o}{L}_v v - \overset{o}{L}_{\dot{w}} \dot{w} - \overset{o}{L}_w w - L_p p - L_q q - \overset{o}{L}_r r + I_x \dot{p} - I_{xz}\dot{r} = \overset{o}{L}_\xi \xi + \overset{o}{L}_\eta \eta + \overset{o}{L}_\zeta \zeta + \overset{o}{L}_\tau \tau \quad (4)$$

$$-\overset{o}{M}_u u - \overset{o}{M}_v v - \overset{o}{M}_{\dot{w}} \dot{w} - \overset{o}{M}_w w - \overset{o}{M}_p p - \overset{o}{M}_q q - \overset{o}{M}_r r + I_y \dot{q} = \overset{o}{M}_\xi \xi + \overset{o}{M}_\eta \eta + \overset{o}{M}_\zeta \zeta + \overset{o}{M}_\tau \tau \quad (5)$$

$$-\overset{o}{N}_u u - \overset{o}{N}_v v - \overset{o}{N}_{\dot{w}} \dot{w} - \overset{o}{N}_w w - \overset{o}{N}_p p - \overset{o}{N}_q q - \overset{o}{N}_r r - I_{xz}\dot{p} + I_z \dot{r} = \overset{o}{N}_\xi \xi + \overset{o}{N}_\eta \eta + \overset{o}{N}_\zeta \zeta + \overset{o}{N}_\tau \tau \quad (6)$$

$$\dot{\varphi} = p + \left(q\sin\varphi + r\cos\varphi\right)\tan\theta \quad (7)$$

$$\dot{\theta} = q\cos\varphi - r\sin\varphi \quad (8)$$

$$\dot{\psi} = \frac{q\sin\varphi + r\cos\varphi}{\cos\theta} \quad (9)$$

where, m is the mass of the UAV, u, v, w are the velocity components in x,y,z axis respectively. η, ξ ,ζ are notations for the control surfaces of elevator, aileron and rudder respectively. X, Y, Z are forces in x,y,z direction and L,M,N are moments in the same axis coordinated . θ, φ, Ψ are the three Euler angles of pitch, roll and yaw respectively. While I_x, I_y and I_z are moment of inertia in roll, pitch and yaw respectively, while I_{xy}, I_{xz} and I_{yz} are the products of inertia in the appropriate axis.

2.1 Aerodynamic Coefficient

The software, Aircraft DIGITAL DATCOM [12] provided the parameters for the aerodynamic model [13] in (10). We recognize that some of these dynamic coefficients may have some limitations. Future work plans to examine the validity of this data. Moreover, for the low subsonic speed, it will be assumed that static aerodynamic coefficients will be assumed constant as a function of velocity, control deflection angles, angle of attack and yaw angles*.* Note that the rudder influence on roll and yaw motion are not provided by DATCOM.

$$\begin{aligned} C_Y &= C_{Y_\beta}\beta + C_{Y_r}\frac{rb}{2V} \\ C_L &= C_{L_\beta}\beta + C_{L_p}\frac{pb}{2V} + C_{L_r}\frac{rb}{2V} + C_{L_{\delta_\xi}}\delta_\xi + C_{L_{\delta_\zeta}}\delta_\zeta \\ C_N &= C_{N_\beta}\beta + C_{N_p}\frac{pb}{2V} + C_{N_r}\frac{rb}{2V} + C_{N_{\delta_\xi}}\delta_\xi + C_{N_{\delta_\zeta}}\delta_\zeta \end{aligned} \quad (10)$$

2.2 Trimming and Linearization

A nonlinear aircraft model built in Simulink was linearized at forward velocity, u=17m/s, pitch angle, θ= 0.0217rad, elevator deflection angle, η = 0.091rad, throttle angle, τ = 0.559rad, aileron and rudder deflections of ξ= 0rad, ζ= 0rad respectively, and altitude of 120m.The simplest form of the equations of motion is taken in the body axis reference frame of the aircraft and assumes an Earth coordinate system. MATLAB scripts for trim and linearization of the 6DoF EoM of the UAV modelled in Simulink, [14] was executed for this study.

To trim or find equilibrium values for a 6DOF equation of motion for a UAV requires a good knowledge of advanced computational techniques. A trim point, also known as an equilibrium point, is a point in the parameter space of a dynamic system at which the system is in a steady state. The trim problem for a UAV can be described as finding a set of suitable input values to satisfy a set of conditions hence, a trim point involves setting of its controls that causes the UAV to fly straight and level in all planes. The suitable input values are the control surface deflections, the thrust setting and the UAV's attitude. The set of conditions are the UAV's accelerations. The variables associated with the trim problems can be divided into three categories:

- Objective variables
- Control variables and
- Flight condition variables.

The objective variables need to be driven towards the specified values, often zero (i.e. steady flight with zero sideslip). The objective parameters are combined in the objective vector *o*, shown as;

$$o = \begin{bmatrix} \dot{u} & \dot{v} & \dot{w} & \dot{p} & \dot{q} & \dot{r} & \beta \end{bmatrix}^T \tag{11}$$

The sideslip angle is also included, since for most cases, there are multiple solutions to the trim problem, each with a different sideslip angle. In the desired solution the sideslip angle should be zero. In that case, the drag is at a minimum. The control parameters are adjusted in order to drive the objective parameters to their specified values. Together, they form the control vector *c*, [15].

$$c = \begin{bmatrix} \delta_e & \delta_a & \delta_r & \tau & \phi & \theta & \psi \end{bmatrix}^T \tag{12}$$

Finally, the 12 states of the 6DOF equation of motion must be initialized; with the initial state conditions. In MATLAB, the *trim* command is used to find equilibrium points. The object of trimming is to bring the forces and moments acting on the UAV into a state of equilibrium. That is the condition when the axial, normal and side forces, and the roll, pitch and yaw moments are all zero.

In MATLAB, the *linmod* [16] command was used to invoke linearization after trimming. The assumption made for decoupling the linear model that will ignore pitch axis effects such as porpoiseing motion but will include the cross coupling effects between the two modes is negligible. These assumptions are;

1. The UAV is designed with conventional control surfaces that do not give significant cross-coupling control between the lateral and longitudinal modes;
2. The UAV is symmetrical about the *xz* plane in which the inertia cross coupling in *xy* (lateral) and *xz* (longitudinal) planes results in minimal cross-coupling between the lateral and longitudinal modes.

Decoupled lateral–directional motion involves roll, yaw and sideslip only. The motion is therefore described by the side force *Y*, the rolling moment *L* and the yawing moment *N* equations only. As no longitudinal motion is involved the longitudinal motion variables *u*, *w* and *q* and their derivatives are all zero. Also, decoupled longitudinal–lateral motion means that the longitudinal aerodynamic coupling derivatives are negligibly small and may be taken as zero whence;

$$\overset{o}{Y}_u = \overset{o}{Y}_{\dot{w}} = \overset{o}{Y}_w = \overset{o}{Y}_q = \overset{o}{L}_u = \overset{o}{L}_{\dot{w}} = \overset{o}{L}_w = \overset{o}{L}_q = \overset{o}{N}_u = \overset{o}{N}_{\dot{w}} = \overset{o}{N}_w = \overset{o}{N}_q = 0. \tag{13}$$

Similarly, since the airframe is symmetric, elevator deflection and thrust variation do not usually cause lateral–directional motion and the coupling aerodynamic control derivatives may also be taken as zero thus;

$$\overset{o}{Y}_\eta = \overset{o}{Y}_\tau = \overset{o}{L}_\eta = \overset{o}{L}_\tau = \overset{o}{N}_\eta = \overset{o}{N}_\tau = 0. \tag{14}$$

The equations of lateral asymmetric motion are therefore obtained by extracting (2), (4),(6),(7) and (9) from the 6DoF equation of motion. This gives;

$$-\overset{o}{Y}_u u + m\dot{v} - \overset{o}{Y}_v v - \overset{o}{Y}_{\dot{w}} \dot{w} - \overset{o}{Y}_w w - \left(\overset{o}{Y}_p + mW_e\right) p - \overset{o}{Y}_q q - \left(\overset{o}{Y}_r - mU_e\right) r - mg\phi\cos\theta_e - mg\psi\sin\theta_e = \overset{o}{Y}_\xi \xi + \overset{o}{Y}_\zeta \zeta \quad (15)$$

$$-\overset{0}{L}_u u - \overset{0}{L}_v v - \overset{0}{L}_{\dot{w}} \dot{w} - \overset{0}{L}_w w - \overset{0}{L}_p p - \overset{0}{L}_q q - \overset{0}{L}_r r + I_x \dot{p} - I_{xz}\dot{r} = \overset{0}{L}_\xi \xi + \overset{0}{L}_\zeta \zeta \quad (16)$$

$$-\overset{o}{N}_u u - \overset{o}{N}_v v - \overset{o}{N}_{\dot{w}} \dot{w} - \overset{o}{N}_w w - \overset{o}{N}_p p - \overset{o}{N}_q q - \overset{o}{N}_r r - I_{xz}\dot{p} + I_z \dot{r} = \overset{o}{N}_\xi \xi + \overset{o}{N}_\zeta \zeta \quad (17)$$

$$\dot{\varphi} = p + \left(q\sin\varphi + r\cos\varphi\right)\tan\theta \quad (18)$$

$$\dot{\psi} = \frac{q\sin\varphi + r\cos\varphi}{\cos\theta} \quad (19)$$

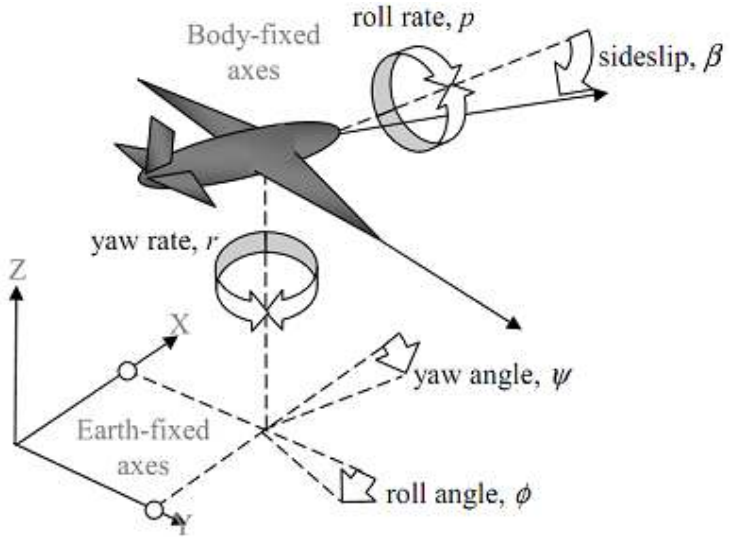

Fig. 2. Perturbed lateral dynamics UAV

In state-space, (15)-(19) can be represented as given with (20) where aileron and rudder serves as the inputs to the system.

$$\begin{bmatrix} \dot{v} \\ \dot{p} \\ \dot{r} \\ \dot{\phi} \\ \dot{\psi} \end{bmatrix} = \begin{bmatrix} y_v & y_p & y_r & y_\phi & y_\psi \\ l_v & l_p & l_r & l_\phi & l_\psi \\ n_v & n_p & n_r & n_\phi & n_\psi \\ 0 & 1 & 0 & 0 & 0 \\ 0 & 0 & 1 & 0 & 0 \end{bmatrix} \begin{bmatrix} v \\ p \\ r \\ \phi \\ \psi \end{bmatrix} + \begin{bmatrix} y_\xi & y_\zeta \\ l_\xi & l_\zeta \\ n_\xi & n_\zeta \\ 0 & 0 \\ 0 & 0 \end{bmatrix} \begin{bmatrix} \xi \\ \zeta \end{bmatrix}, \quad (20)$$

The lateral–directional state equation (20) is reduced from fifth order to fourth order as given in (22). In this case the derivatives are referred to aeroplane wind axes rather than body axes and will generally have slightly different values from the former. It can be shown that in a lateral perturbation the sideslip angle β is given by

$$\beta \approx \tan^{-1}\left(\frac{v}{u_0}\right) = \frac{v}{u_0}, \tag{21}$$

and the lateral small perturbation equations can be modified to incorporate sideslip angle β in the output equation or alternatively, it may replace lateral velocity v in the state equation. When the output equation is augmented, the lateral state equations may be written as:

$$\begin{bmatrix} \dot{\beta} \\ \dot{p} \\ \dot{r} \\ \dot{\phi} \end{bmatrix} = \begin{bmatrix} y_v & y_p/V_0 & y_r/V_0 & y_\phi/V_0 \\ l_v V_0 & l_p & l_r & l_\phi \\ n_v V_0 & n_p & n_r & n_\phi \\ 0 & 1 & 0 & 0 \end{bmatrix} \begin{bmatrix} \beta \\ p \\ r \\ \phi \end{bmatrix} + \begin{bmatrix} y_\xi/V_0 & y_\zeta/V_0 \\ l_\xi & l_\zeta \\ n_\xi & n_\zeta \\ 0 & 0 \end{bmatrix} \begin{bmatrix} \xi \\ \zeta \end{bmatrix}, \tag{22}$$

where, y_v, y_p, y_r, and $y_\varnothing$ are the dimensionless stability aerodynamic derivatives with respect to the state variables, while y_ζ, and y_ξ are the dimensionless control aerodynamic derivatives. ξ and ζ are the aileron and rudder input control signal. For this study, our lateral model is;

$$\dot{x} = \begin{bmatrix} -0.86 & 0.93 & -16.76 & 9.69 \\ -2.76 & -15.83 & 3.31 & 0 \\ 1.67 & 0.51 & -2.73 & 0 \\ 0 & 1 & 0.07 & 0 \end{bmatrix} x + \begin{bmatrix} 0.05 & 5.12 \\ -154 & -4.93 \\ 11.30 & -80.70 \\ 0 & 0 \end{bmatrix} \begin{bmatrix} \xi \\ \zeta \end{bmatrix} \tag{23}$$

$$y = \begin{bmatrix} 0.59 & 0 & 0 & 0 \end{bmatrix} \begin{bmatrix} \beta \\ p \\ r \\ \phi \end{bmatrix} \tag{24}$$

The steady state values (DC gains) to a unit step aileron and rudder input are computed as;

$$k_L = -CA^{-1}B = \begin{bmatrix} -87.0 & -85.6 \end{bmatrix} \begin{bmatrix} \xi \\ \zeta \end{bmatrix} \tag{25}$$

Transfer functions were extracted from the state-space model using the MATLAB command *ss2tf*, Maple was then used to factor the numerator and denominator. These transfer functions are as given in (26) and (27), while their numerical open-loop responses to a step signal are depicted in Fig. 3.

$$G_L(s)_{\beta_\xi} = \frac{\beta(s)}{\xi(s)} = \frac{0.00295(s+9.45)(s+1.16)(s-6644.5)}{(s+15.78)(s+0.00512)(s^2+3.64s+30.56)}, \tag{26}$$

$$G_L(s)_{\beta_\zeta} = \frac{\beta(s)}{\zeta(s)} = \frac{0.3021(s+266.19)(s+15.80)(s-0.17)}{(s+15.78)(s+0.00512)(s^2+3.64s+30.56)}, \tag{27}$$

In Maple, the analytical open-loop step response [17] for the sideslip angle with aileron and rudder inputs are given in (28) and (29) respectively.

$$\beta_{\xi}(t) = -86.97 - 0.03e^{-15.57t} + (0.19 + 0.06i)e^{(-1.82-5.22i)t} + (0.19 - 0.059i)e^{(-1.82+5.22i)t} + 86.62e^{-0.0051t} \quad (28)$$

$$\beta_{\zeta}(t) = -85.6 - 0.0007e^{-15.57t} + (-1.34 - 0.4i)e^{(-1.82-5.22i)t} + (-1.34 - 0.4i)e^{(-1.82+5.22i)t} + 88.29e^{-0.0051t} \quad (29)$$

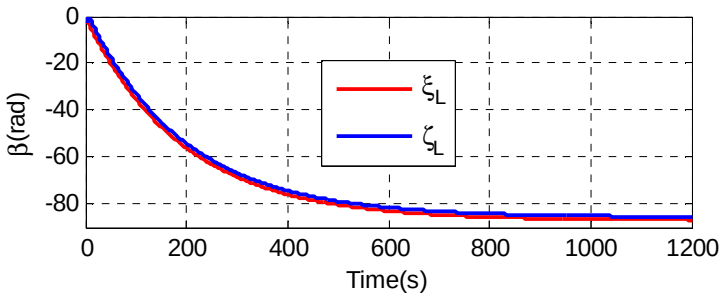

Fig. 3. Open loop response for sideslip angle and roll rate

Open-loop bode plot for the transfer function in (26) and (27) are shoe in Fig. 4

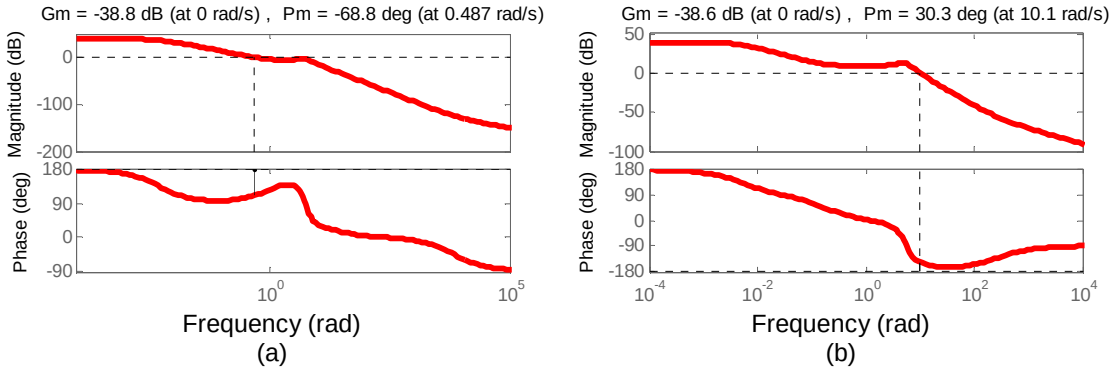

Fig. 4. Bode plots for sideslip angle transfer functions with (a) aileron (b) rudder inputs

The lateral–directional characteristic polynomial for a classical aeroplane is fourth order; when equated to zero, defines the characteristic equation [18] which may be written as

$$As^4 + Bs^3 + Cs^2 + Ds + E = 0. \quad (30)$$

The expression (30) most commonly factorises into two real roots and a pair of complex roots which are most conveniently written as

$$s\left(1+(1/T_s)\right)\left(1+(1/T_r)\right)\left(s^2 + 2\zeta_L\omega_L s + \omega_L^2\right) = 0. \quad (31)$$

Here, Maple was used to obtain the characteristics equation in (32) from the state space model in (23) and using the *factor* command in Maple, we obtained the expression in (33).

$$\lambda^4 + 19.42\lambda^3 + 88.05\lambda^2 + 482.67\lambda + 2.47. \quad (32)$$

$$(s+15.78)(s+0.00512)\left(s^2 + 3.64s + 30.56\right) \quad (33)$$

The distinctive roots of the lateral model are deduced to be

$$\lambda_L = \begin{bmatrix} -15.78 \\ -1.82 \pm 5.22i \\ -0.0051 \end{bmatrix}, \quad (34)$$

The eigenvalues and corresponding eigenvector magnitude of the lateral model are described in Table 2. Also, associated with the eigenvalues and the eigenvector magnitudes are the 3 distinct modes of the lateral dynamics.

Table 2. Mode, eigenvalues and eigenvector magnitude

Variable	Dutch roll (-1.82± 5.22*i*)	Roll (-15.78)	Spiral (-0.0051)
β	0.9434	0.0567	0.6131
p	0.1745	0.9959	0.0295
r	0.1245	0.0317	0.3702
φ	0.0992	0.0630	0.6973

The eigenvector magnitudes, show that the roll mode is dominate in roll rate *p.* Spiral mode dominates in roll attitude response *φ*. And Dutch Roll mode dominates changes in sideslip angle.

Comparing terms between (30) and (32), approximate values for the roll mode and spiral mode time constants are given by

$$T_r \cong \frac{A}{B} = \frac{1}{19.42} = 0.05\text{s} \tag{35}$$

$$T_s \cong \frac{D}{E} = \frac{482.67}{2.47} = 195.4\text{s} \tag{36}$$

The natural frequency and damping ratio of the Dutch Roll mode in the lateral dynamics are obtaining by comparing terms also in (31) and (33), this gives the following;

$$\omega_L = \sqrt{30.5628} = 5.53\text{sec}^{-1} \tag{37}$$

$$\zeta_L = \frac{3.64}{2\omega_L} = 0.33 \tag{38}$$

The period of the Dutch Roll mode in the lateral dynamics model is given in (39) and the number of cycles to damp to half amplitude in (40)

$$T_L = \frac{2\pi}{\omega_L\sqrt{1-\zeta^2}} = \frac{2\pi}{5.53\sqrt{1-0.3316^2}} = 1.2\text{sec} \tag{39}$$

$$N_{1/2_L} = \frac{\ln 2}{2\pi}\frac{\sqrt{1-\zeta^2}}{\zeta} = \frac{\ln 2}{2\pi}\frac{\sqrt{1-0.3316^2}}{0.3316} = 0.296 \tag{40}$$

2.3 Approximation to Dutch Roll Mode

Assuming that Dutch rolling motion involves no rolling motion at all, and is based on the fact that the mode is primarily a yawing oscillation and aerodynamic coupling causes rolling motion as a secondary effect. Hence, this Thus, this assumption holds;

$$\dot{p} = p = \dot{\phi} = \phi = 0. \tag{41}$$

Considering that the Dutch roll mode consists primarily of sideslip angle and yaw motion, then we can neglect the rolling moment equation. With this assumption, (23) reduces to;

$$\begin{bmatrix}\dot{\beta}\\ \dot{r}\end{bmatrix} = \begin{bmatrix}y_v & y_r\\ n_v & n_r\end{bmatrix}\begin{bmatrix}\beta\\ r\end{bmatrix} + \begin{bmatrix}y_\xi & y_\zeta\\ n_\xi & n_\zeta\end{bmatrix}\begin{bmatrix}\xi\\ \zeta\end{bmatrix} = \begin{bmatrix}-0.86 & -16.76\\ 1.67 & -2.73\end{bmatrix}x + \begin{bmatrix}0.05 & 5.12\\ 11.3 & -80.7\end{bmatrix}\begin{bmatrix}\xi\\ \zeta\end{bmatrix} \tag{42}$$

The roots of the approximated Dutch roll model are given in (43) and steady state values for sideslip angle are expressed in (44)

$$\lambda_{DR} = \left[-1.795 \pm 5.21i\right], \tag{43}$$

$$k_{DR} = -CA^{-1}B = \begin{bmatrix}-6.24 & 45.04\end{bmatrix}\begin{bmatrix}\xi\\ \zeta\end{bmatrix} \tag{44}$$

The characteristic equation for the DR approximation is given in (45) and its general for is given in (46).

$$\lambda^2 + 3.59\lambda + 30.3370 = 0 \tag{45}$$

$$s^2 + 2\zeta_{DR}\omega_{DR}s + \omega_{DR}^2 = 0 \quad (46)$$

Hence we can go ahead to compute the DR approximation model's natural frequency and damping ratio as follows:

$$\omega_{DR} = \sqrt{30.337} = 5.51\text{sec}^{-1} \quad (47)$$

$$\zeta_{DR} = \frac{2\zeta_{DR}\omega_{DR}}{2\omega_{DR}} = \frac{3.59}{11.02} = 0.33 \quad (48)$$

The period of the Dutch Roll mode from the DR approximated model is given in (49) and the number of cycles to damp to half amplitude in (50)

$$T_{DR} = \frac{2\pi}{\omega_{DR}\sqrt{1-\zeta_{DR}^{\ 2}}} = \frac{2\pi}{5.51\sqrt{1-0.33^2}} = 1.2\,\text{sec} \quad (49)$$

$$N_{1/2_L} = \frac{\ln 2}{2\pi}\frac{\sqrt{1-\zeta_{DR}^{\ 2}}}{\zeta_{DR}} = \frac{\ln 2}{2\pi}\frac{\sqrt{1-0.33^2}}{0.33} = 0.32 \quad (50)$$

For aileron and rudder inputs to sideslip angle, the transfer functions for the Dutch roll approximations are given as;

$$G_{DR}(s)_{\beta_\xi} = \frac{\beta(s)}{\xi(s)} = \frac{0.05s - 189.3}{s^2 + 3.59s + 30.34}, \quad (51)$$

$$G_{DR}(s)_{\beta_\zeta} = \frac{\beta(s)}{\zeta(s)} = \frac{5.12s + 1367}{s^2 + 3.59s + 30.34}, \quad (52)$$

The analytical forms of the sideslip angle step response to aileron and rudder inputs in the DR approximation are given in (53) and (54),while the numerical responses is depicted in Fig. 5.

$$\beta_\xi(t) = -6.24 + 3.04\times10^{-9}e^{-1.795t} + \left(7.11\times10^{8}\sin(5.21t) + 2.05\times10^{9}\cos(5.21t)\right) \quad (53)$$

$$\beta_\zeta(t) = 45.06 - 3.64\times10^{-9}e^{-1.795t} + \left(3.98\times10^{9}\sin(5.21t) + 1.24\times10^{10}\cos(5.21t)\right) \quad (54)$$

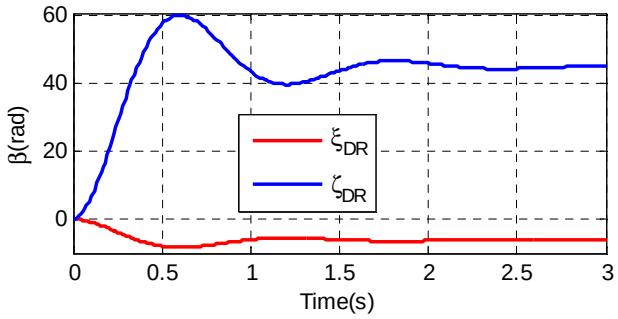

Fig. 5. DR sideslip angle response to a step signal

Open-loop bode plot for the sideslip angles transfer functions given in (45), (46) are given in Fig. 6.

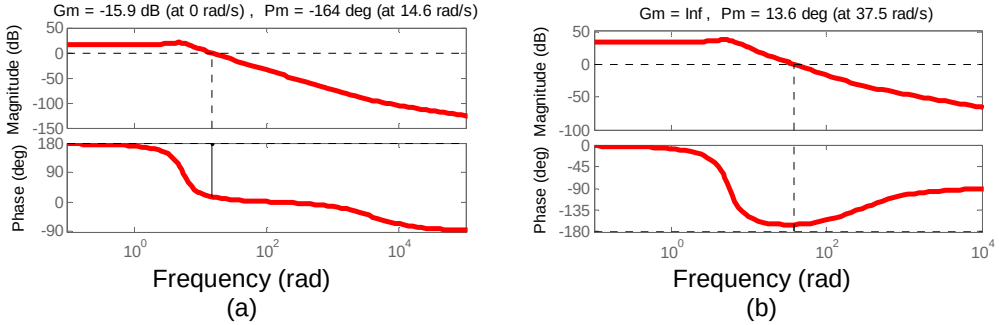

Fig. 6. Bode plots for DR model sideslip angle transfer functions with (a) aileron (b) rudder inputs

Table 3 captures the numerical values of all poles and zeros of the transfer functions in the study.

Table 3. Poles and zeros of transfer functions

S/N	Plant	Poles	Zeros
1.	$G_L(s)_{\beta_\xi}$	-15.78,-1.82±5.22*i*, -0.0051	6644.5,-9.4,-1.2
2.	$G_L(s)_{\beta_\zeta}$	-15.78,-1.82±5.22*i*, -0.0051	-266.2,-15.8, 0.17
3.	$G_{DR}(s)_{\beta_\xi}$	-1.82±5.22*i*	3786
4.	$G_{DR}(s)_{\beta_\zeta}$	-1.82±5.22*i*	-266.9

2.4 Actuator Dynamics

For simplicity, a linear second order model of an actuator is employed with the following dynamic characteristics; natural frequency of 150*rad* /s, damping ratio of 0.7, and an initial condition of zero. Its transfer function is given as;

$$H(s) = \frac{\omega_n^2}{s^2 + 2\xi\omega_n + \omega_n^2} \quad (55)$$

3. AUTOPILOT DESIGN WITH PROPORTIONAL-INTEGRAL-DERIVATIVE (PID) CONTROL

In this section, the autopilot system in a typical UAV is described together with the PID control algorithm intended for the system control loop.

3.1 Autopilot

An autopilot is a MEMs system used to guide the UAV without assistance from human operators, which consists of both hardware and its supporting software. A UAV autopilot has a close-loop control system, which comprises of two parts: the state observer and the controller. It has two fundamental functions: state estimation and control inputs generation based on the reference paths and the current states. The primary objective of UAV autopilot systems is to consistently guide UAVs to follow reference paths, or navigate through some *waypoints* [19]. Here we chose to control the sideslip angles of the UAV for future implementation of the obtained PID control gains in an autopilot system.

3.2 PID Control

Proportional-Integral-Derivative (PID) control is a classical single-input-single-output control algorithm. They have proven to be robust in the control of many important applications. The simplicity of these controllers is also their weakness, since it limits the range of plants that they can control satisfactorily. Indeed, there exists a set of unstable plants which cannot even be stabilized with any member of the PID family [20]. In other to design a PID controller, the mathematical model of the system to be controlled must be in transfer function. The aim of a PID controller is to make the error signal, i. e., the difference between the reference signal and the measured signal, as small as possible (go to zero with time) [21,22]. This is expressed mathematically as

$$\lim_{t\to\infty} e = \lim_{t\to\infty} r - y \to 0 \quad (56)$$

Where, *r* is the reference signal and *y* is the measured signal from the sensor and for this study, sensor gain is taken as unity.

Mathematically, the PID controller designed in this study is described as:

$$[\xi \quad \zeta]^T = K_p e(t) + K_i \int_0^t e(\tau)d\tau + K_d \frac{d}{dt} e(t), \quad (57)$$

where K_p, K_i and K_d represent proportional, integral and derivative gains respectively, and ξ, ζ are the aileron and rudder input signals.

The PID control design objective in this study is to control the sideslip angle to meet the following design specifications;

- Settling time less than 3 seconds;
- Rise time less than 0.1 seconds;
- Percentage overshoot less than 10 per cent
- Gain margin, at least 3db

- Phase margin at least 30°
- Bandwidth of about 150 rads/s

Hence, with the transfer functions of interest at hand, a set-point tracking PID control scheme was modelled in MATLAB/Simulink as shown in Fig. 7, [23]. Simulation results are shown in Fig. 8.

The pre-modelled PID block that comes with MATLAB/Simulink 2014a, was used to tune the PID gains. When implemented in a design as shown in Fig. 8, it linearizes the system and comes up with optimum values for k_d, k_p, and k_i. A window is immediately launched after the tuning and system characteristics (Table 4) are displayed. If further tuning is required, this is done directly on the pop-up window; either to make the tuned response faster or slower. While this is done, controller characteristics are also automatically modified.

4. DISCUSSION OF RESULTS

The Dutch Roll (DR) mode in (42) is a reduced form of the full lateral model of the UAV in (23). The eigenvalues identified as those of the DR mode in the full lateral model in (34), are the same with those in the reduced model in (43). Both systems *DC* gains (steady-state values) vary as presented in (25), and (44). Hence, the open-loop step responses of the two systems are also different. These were numerically computed in MATLAB 2014a and depicted in Figs.3 and 5. It is pertinent to note that steady-state values with respect to aileron and rudder in the lateral dynamics have close magnitude values and on the same side of the Cartesian

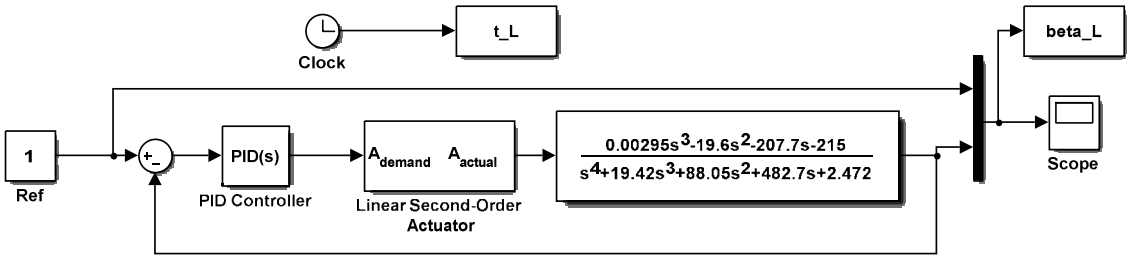

Fig. 7. PID controller design for lateral dynamics sideslip angle in MATLAB/Simulink

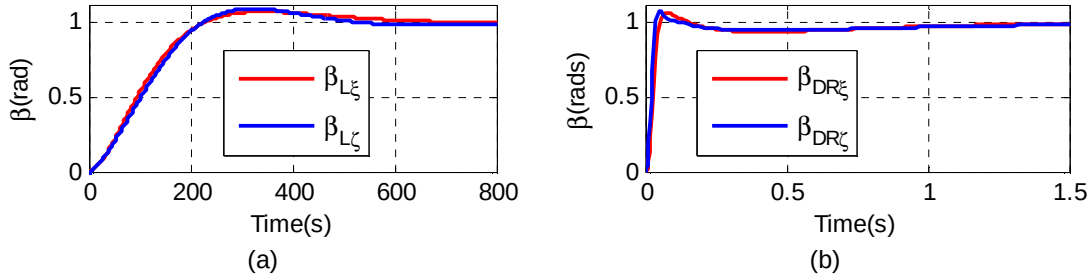

Fig. 8. Closed-loop *step* responses of PID controlled sideslip angles

Table 4. Roll and sideslip angle designed PID controller characteristics

S/N	Plant	Controllers				Transient response			Stability	
		P	*I*	*D*	*N*	t_r(s)	*ts(s)*	*PO(%)*	GM(db)	PM(deg)
1	$G_L(s)_{\beta_\xi}$	-0.01	-0.00	0.43	0.03	153	576	7.40	82.60, @5.41rads/s	64.7^0 @0.009rads/s
2	$G_{DR}(s)_{\beta_\xi}$	-1.21	-2.11	-0.17	359	0.03	1.13	7.13	12.3 @115rads/s	60.0^0 @34.2rads/s
3	$G_L(s)_{\beta_\zeta}$	-0.01	-0.00	1.30	0.01	159	486	9.30	34.10 @1.04rads/s	60.0^0 @0.009rads/s
4	$G_{DR}(s)_{\beta_\zeta}$	0.22	0.29	0.03	260	0.02	1.25	8.57	12.6 @147rads/s	60.0^0 @47.8rads/s

coordinate (positive or negative). For the DR model, these values are widely apart and on opposite side of the Cartesian coordinate.

Analytical open-loop step response was computed using Maple 18, for all transfer functions as shown in (28), (29), (53) and (54). This was necessary to verify results of eigenvalues and DC gains obtained in MATLAB. Also, Maple's symbolic forms of the step response give a single expression depicting system eigenvalues, decaying terms, and steady state values for each input signals.

The natural frequencies, damping ratio, period and number of cycle to damp to half amplitude of the Dutch roll mode in the lateral dynamics i.e., (37), (38), (39), (40) are about the same with those of the reduced lateral model in the Dutch roll approximation, i.e., (47), (48), (49), (50).

The stability of any systems depends only on the poles of the system. All poles of the transfer functions are stable. Poles must be in the left half plane (negative) for the system to be stable. This fact is evident from (34) and (43) and also, depicted in the analytical expressions, (28), (29), (53) and (54).

Open-loop bode plot of $G_L(s)_{\beta\xi}$,$G_L(s)_{\beta\zeta}$ (Fig. 4) and $G_{DR}(s)_{\beta\xi}$ (Fig. 6a), suggest unstable system dynamics hence, the need to design controllers is inevitable. But for $G_L(s)_{\beta\zeta}$, its open-loop bode plot suggest a stable system. Stability of a system in open-loop does not guarantee closed-loop system stability especially in an autopilot system where a reference signal needs to be tracked.

The transient response characteristics of a closed-loop dynamic system (plant with controller) described by transfer functions depends on the poles and zeros of the plant. In this study, $G_{DR}(s)_{\beta\zeta}$ is the only *minimum phased* plant, as shown in Table 3. Hence, its phase response is restricted within 0 degrees to -90 degrees and the amplitude (GM) response is 12.6db or unique for a frequency of 146rads/s (Table 4). The rest are *Non minimum phase* systems. The range of phase angle of these systems phase transfer function is greater than 90 degrees. Also, the *non-minimum phase* systems are slow in response because of their faulty behaviour at the start of the response. This is shown in their *rise time*, for the *minimum phase* plant $G_{DR}(s)_{\beta\xi}$ it has a *rise time*, t_r= 0.02 which is the lowest compared to the others in Table 4.

The basic essence of a control algorithm like the PID is to make an unstable plant stable by moving its poles to the left hand plane and ensure that those with stable poles have acceptable closed-loop stability margins and appreciable time response characteristics. In this study, all PID controlled plants have appreciable transient characteristics and stability margins except $G_L(s)_{\beta\xi}$ and $G_L(s)_{\beta\zeta}$; plagued with a *rise time* greater than 100s and *settling time* above 400s (Table 4).

5. CONCLUSION

To control the sideslip angles of a UAV, we obtained a lateral dynamics mathematical model for a mini-UAV flying at a fairly constant velocity at Mach 0.3. Transfer function describing sideslip angle were obtained after converting the UAV linearized state-space model to transfer function in MATLAB/Simulink. The lateral model was compared with it reduced form of DR approximation in all dynamic characteristics and disparity were found only in steady state values and open-loop step responses of both models. Non- minimum phased plants were observed to lag the minimum phased plants in *rise time* after PID controllers were designed. From the standpoint of our control design objective, the sideslip angle controllers from the DR model met all design objectives. Those from the lateral dynamics model failed to meet the time response characteristic design objectives of *rise time* and *settling time*.

To an extent, this shows the limitation of SISO control algorithms over Multiple-Input-Multiple-Output (MIMO) control algorithms. In the former cross-coupling system dynamics effect are neglected and might have marred the control effort of the PID control algorithm in the plant dynamics of $G_L(s)_{\beta\xi}$ and $G_L(s)_{\beta\zeta}$. Hence, control gains from such plants implemented in an autopilot system will jeopardize the mission of our UAV. It is pertinent to note that UAV or aircraft flying at supersonic speed with velocity that are not constant are bound to have different behaviors and may obviously require additional analysis and study.

COMPETING INTERESTS

Authors have declared that no competing interests exist.

REFERENCES

1. Reed Siefert Christiansen. Design of an Autopilot for Small Unmanned Aerial

Vehicles. M.S. thesis, Electrical and Computer Engineering, Brigham Young University. 2004;2-4.

2. Pike J. (2003), "Dragon Eye" Intelligence Resources. 2000. GlobalSecurity.org. Available:http://www.globalsecurity.org/intell/systems/dragon-eye.htm
3. Erickson GE, et al. Experimental investigation of the F/A-18 vortex flows at subsonic through transonic speeds. Presented at Appl. Aerodyn. Conf., 7 th, AIAA Pap. 89–2222, Seattle, WA; 1989.
4. Falkner VM. The calculation of aerodynamic loading on surfaces of any shape. ARC R&M 1910; 1943.
5. Cobleigh BR. High-angle-of-attack yawing moment asymmetry of the X-31 aircraft from flight test. Presented at Appl. Aerodyn. Conf., 12 th, AIAA Pap. 94–1803, Colorado Springs, CO; 1994.
6. Turkoglu K, Ozdemir U, Nikbay M, et al. PID parameter optimization of an UAV longitudinal flight control system. World Academy of Science, Engineering and Technology, International Journal of Mechanical, Industrial Science and Engineering. 2008;2(9):24-29.
7. Kada B, Ghazzawi Y. Robust PID controller design for an UAV flight control system, in Proceedings of the World Congress on Engineering and Computer Science 2011 Vol II, WCECS 2011, San Francisco, USA, October 19-21; 2011.
8. Vaglienti B, Hoag R, Niculescu M. Piccolo System User Guide, Cloud Cap Technology, 1.3.2 edition, April 2008. Available:http://www.cloudcaptech.com/resources_autopilots.shtm
9. MicroPilot, MP2028g Installation and Operation; 2005. Available:http://www.micropilot.com/Manual-MP2028.pdf
10. Bennett S. Nicolas Minorsky and the Automatic Steering of Ships; 1984.
11. Cook M. Flight Dynamics Principles, Elsevier Ltd., 2nd ed; 2007.
12. Datcom+ Pro Users Manual Version 3.1; 2011. Holy Cows, Inc. 3757 Lake Drawdy Driv Orlando, FL 32820
13. Jacek A Goszczynski. Practical aspects of identification of the aerodynamic characteristics. Journal of Theoritical and Applied Mechanics. 2006;44(1):31-50. Warsaw.
14. Murch A. UAV Research Group. Available:http://www.uav.aem.umn.edu
15. Kalthof RLC. Multibody dynamics modelling of flexible aircraft flight dynamics. Master of Science Thesis, Delft University of Technology Department of Flight Performance and Propulsion; 2014.
16. Control System Toolbox™ User's Guide R2014a of MATLAB © Copyright 2001–2014 by The MathWorks, Inc
17. Frank Garvan. The Maple Book'. Chapman & Hall/CRC; 2002. ISBN 1-58488-232-8.
18. Ashish Tewari. Advance control of aircraft, spacecraft and rockets. John Wiley & Sons, Ltd; 2011. ISBN 978-0-470-74563-2.
19. HaiYang Chao, et al. Autopilots for small unmanned aerial vehicles: A survey. International Journal of Control, Automation, and Systems. 2010;8(1):36-44.

    DOI: 10.1007/s12555-010-0105-z

    Available:http://www.springer.com/12555
20. Graham C Goodwin, Stefan F Graebe, Mario E Salgado. Control System Design; 2000.
21. Niler Lwin, Hia Myo Tun. Implementation of flight control sytem based on Kalman and PID controller for UAV. International Journal of Scientific & Technology Research. 2014;3(4). ISSN 2277-8616. Available:www.ijstr.org
22. Roy Langton. Stability and Control of Aircraft Systems Introduction to Classical Feedback Control'. John Wiley & Sons Inc., USA; 2006. ISBN-13 978-0-470-01891-0 (HB)
23. Roy Langton. Stability and Control of Aircraft Systems. John Wiley & Sons Inc., 111 River Street, Hoboken, NJ 07030, USAISBN-13 978-0-470-01891-0 (HB); 2006.

Peer-review history:
The peer review history for this paper can be accessed here:
http://sciencedomain.org/review-history/12604